

# BMRL: Bi-Modal Guided Multi-Perspective Representation Learning for Zero-Shot Deepfake Attribution

Yaning Zhang  
zhangyaning0321@163.com  
Qilu University of Technology  
(Shandong Academy of Sciences)  
Jinan, China

Jiahe Zhang  
zhangjiahe00600@163.com  
Shandong University of Science and  
Technology  
Jinan, China

Chunjie Ma  
machunjie@qlu.edu.cn  
Qilu University of Technology  
(Shandong Academy of Sciences)  
Jinan, China

Weili Guan  
guanweili@hit.edu.cn  
Harbin Institute of Technology  
(Shenzhen)  
Shenzhen, China

Tian Gan  
gantian@sdu.edu.cn  
Shandong University  
Qingdao, China

Zan Gao  
zangaonsh4522@gmail.com  
Qilu University of Technology  
(Shandong Academy of Sciences)  
Jinan, China

## Abstract

The challenge of tracing the source attribution of forged faces has gained significant attention due to the rapid advancement of generative models. However, existing deepfake attribution (DFA) works primarily focus on the interaction among various domains in vision modality, and other modalities such as texts and face parsing are not fully explored. Besides, they tend to fail to assess the generalization performance of deepfake attributors to unseen generators in a fine-grained manner. In this paper, we propose a novel **bi**-modal guided **multi**-perspective **representation learning** (BMRL) framework for **zero-shot deepfake attribution** (ZS-DFA), which facilitates effective traceability to unseen generators. Specifically, we design a multi-perspective visual encoder (MPVE) to explore general deepfake attribution visual characteristics across three views (i.e., image, noise, and edge). We devise a novel parsing encoder to focus on global face attribute embeddings, enabling parsing-guided DFA representation learning via vision-parsing matching. A language encoder is proposed to capture fine-grained language embeddings, facilitating language-guided general visual forgery representation learning through vision-language alignment. Additionally, we present a novel deepfake attribution contrastive center (DFACC) loss, to pull relevant generators closer and push irrelevant ones away, which can be introduced into DFA models to enhance traceability. Experimental results demonstrate that our method outperforms the state-of-the-art on the ZS-DFA task through various protocols evaluation.

## CCS Concepts

• **Security and privacy** → **Human and societal aspects of security and privacy**; • **Computing methodologies** → **Computer vision problems**.

Permission to make digital or hard copies of all or part of this work for personal or classroom use is granted without fee provided that copies are not made or distributed for profit or commercial advantage and that copies bear this notice and the full citation on the first page. Copyrights for components of this work owned by others than the author(s) must be honored. Abstracting with credit is permitted. To copy otherwise, or republish, to post on servers or to redistribute to lists, requires prior specific permission and/or a fee. Request permissions from [permissions@acm.org](mailto:permissions@acm.org).  
*Conference'17, Washington, DC, USA*

© 2025 Copyright held by the owner/author(s). Publication rights licensed to ACM.  
ACM ISBN 978-x-xxxx-xxxx-x/YYYY/MM  
<https://doi.org/10.1145/nnnnnnn.nnnnnnn>

## Keywords

Deepfake attribution, zero-shot learning, vision-language model, multi-perspective fusion.

## ACM Reference Format:

Yaning Zhang, Jiahe Zhang, Chunjie Ma, Weili Guan, Tian Gan, and Zan Gao. 2025. BMRL: Bi-Modal Guided Multi-Perspective Representation Learning for Zero-Shot Deepfake Attribution. In . ACM, New York, NY, USA, 11 pages. <https://doi.org/10.1145/nnnnnnn.nnnnnnn>

## 1 Introduction

With the proliferation of advanced generative frameworks, including generative adversarial networks (GANs) [5] and diffusion models [14], maliciously fabricated deepfake content on social platforms has raised significant concerns over facial integrity and personal privacy [19]. As a result, tracing the source of deepfakes has become a critical and urgent issue. Deepfake attribution (DFA) has been introduced to address this challenge, aiming to identify and attribute forged faces using deep learning-based methods. Although current DFA techniques [25, 34] have made significant progress, they predominantly assume a closed-world setting where the training and testing sets share identical category distributions. This assumption limits their applicability in open-world scenarios, where novel forgery attacks continuously emerge. To overcome this limitation, open-world deepfake attribution (OW-DFA) leverages unlabeled data in open-world contexts, to enhance attribution performance for forgery faces created by both seen and unseen generators. However, most DFA models [27, 28] focus solely on the interaction between image and frequency information within the visual modal, neglecting other modalities such as fine-grained text and face parsing, which may hinder generalization to unseen generators. For instance, DNA-Det [34] identifies globally consistent forgery features using the image modality for GAN architecture attribution. CPL [28] captures both local and global forgery features in vision modality, achieving superior attribution performance for GAN-generated face images. MPSSL [27] further explores multi-scale image and frequency relationships among samples, enabling the attribution of both GAN and diffusion-generated face images [2]. However, they struggle to evaluate the generalization to unseen generators in a fine-grained manner.

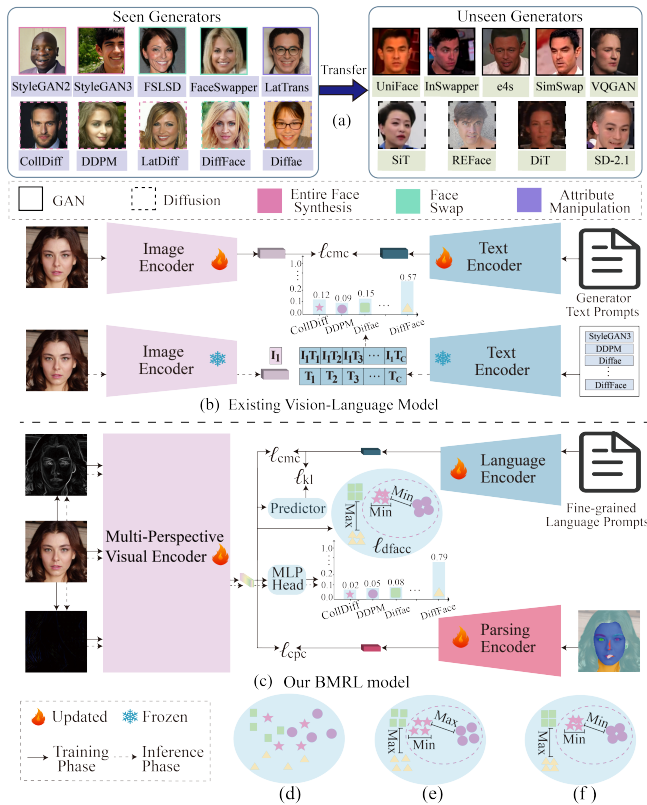


**Figure 1: (a) In ZS-DFA tasks, training and testing datasets are derived from distinct domains, with generators in the testing dataset being unseen during the training stage. (b) The existing vision-language foundation model CLIP. (c) The proposed BMRL framework. (d) Original DFA feature space. (e) DFA feature space supervised by vanilla contrastive center loss. (f) DFA feature space supervised by our DFACC loss.**

To alleviate the limitations, we introduce a novel task, namely, zero-shot deepfake attribution (ZS-DFA), which aims to identify the source generator of a deepfake image without prior exposure to its samples. It is critical for digital forensics, enabling the traceability of synthetic media in real-world scenarios where the source model is unknown. Specifically, as shown in Figure 1 (a), ZS-DFA encompasses about 20 advanced generators, categorized into three manipulations such as entire face synthesis (EFS), face swap (FS), and attribute manipulation (AM). The main challenge of ZS-DFA is how to design an attributor to mine general forgery traces synthesized by seen generators, to enhance the attribution performance for fake faces created by unseen ones.

Inspired by the contrastive language-image pre-training (CLIP) model [21] which excels at zero-shot learning, we propose a bi-modal guided multi-perspective representation learning (BMRL) framework. Unlike CLIP which only focuses on image and text modalities for zero-shot classification in general natural image scenarios, our BMRL model introduces fine-grained text and face parsing modalities, to enhance the learning of multiple-perspective (i.e., image, noise, and edge) visual features via cross-modality matching and cross-perspective alignment, to achieve ZS-DFA. Specifically, our BMRL method differs from CLIP in the following points (See

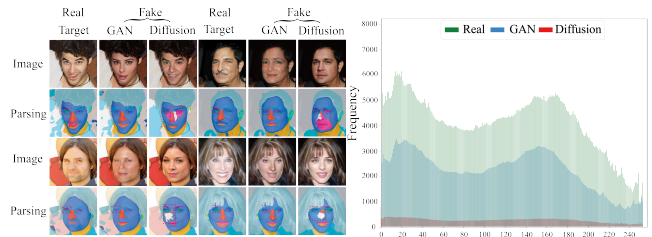


**Figure 2: Illustration of the face attribute-sensitive trait. Left: The visualization of real, GAN, and diffusion face parsing images. Right: The feature distribution histogram of real, GAN, and diffusion face parsing images.**

Figure 1): First, since most face manipulations such as FS struggle to preserve facial attributes of the source image like eyebrows and eyes [19], as shown in Figure 2, we employ a face parser [32] to generate parsing images to focus on different facial attribute regions. We observe that there are significant differences between pristine and forged face parsing images (See Figure 2). Specifically, authentic face parsing images exhibit more precise attribute areas (e.g., eyes and eyebrows) than forged ones. Besides, parsing images derived from GAN-generated faces retain more accurate semantic attributes than those extracted from diffusion faces. Based on the observation, we propose a parsing encoder (PE) to capture global face parsing features, guiding our BMRL model to learn discriminative and general deepfake attribution embeddings. Second, we design a multi-perspective visual encoder (MPVE) to explore global multi-view (i.e., image, edge, and noise) forgery representations, as there are significant discrepancies between real and fake images in both edge and noise views [36, 37]. We also propose a language encoder to extract fine-grained language attribution embeddings for comprehensive vision-language matching. Finally, to enhance the ZS-DFA capability, we design a novel deepfake attribution contrastive center loss (See Figure 1 (f)). Unlike the vanilla contrastive center loss [20] which enforces intra-generator compactness and inter-generator separability, our loss minimizes the distance between samples within the generator, while bringing related samples across generators closer and pushing unrelated ones farther apart. In summary, the contributions of our work are as follows:

- To the best of our knowledge, our work is the first to achieve excellent zero-shot deepfake attribution performance. We propose a novel bi-modal guided multi-perspective representation learning (BMRL) model, which introduces the fine-grained text and face parsing modalities to boost the learning of visual forgery features across image, noise, and edge views.
- We design an innovative parsing encoder, which explores diverse and global parsing forgery patterns, to guide the model to extract complementary and generalized attribution representations through vision-parsing matching.
- We propose a plug-and-play deepfake attribution contrastive center criterion to realize flexible intra-generator compactness and inter-generator separability, which could be integrated into any deepfake attributors to improve traceability performance.

## 2 Related Work

### 2.1 Deepfake Attribution

Deepfake attribution aims to identify the source of a deepfake image through deep learning-based models, which is a challenging task due to the sophistication and realism of deepfake technology. Most existing efforts [4, 25, 28, 34] focus on attributing GAN-generated content, with little attention given to more recent advanced generators like diffusion models. DNA-Det [34] is designed to capture globally consistent architecture traces, via pre-training on image transformation classification and patch-based contrastive learning. Sun et al. [28] propose a contrastive pseudo learning (CPL) framework for open-world deepfake attribution tasks, which evaluates attribution performance against various GAN-generated fake face images. To address the limitation, MPSSL [27] models global, multi-scale local image, and frequency relations among samples to attribute fake images generated by various diffusion models. DE-FAKE [25] employs the CLIP model to detect and attribute fake images created by diffusion text-to-image generation models. However, they struggle to fully explore fine-grained text and vision modalities, which may lead to poor generalization to unseen generators. By contrast, we conduct the bi-modal (i.e., parsing and text) guided multi-perspective (i.e., image, edge, and noise) visual forgery representation learning, to realize ZS-DFA.

### 2.2 Zero-Shot Learning

Zero-Shot learning (ZSL) enables a model to recognize and classify instances from unseen classes during the training phase. Traditionally, ZSL [16, 26] for image classification relies on learning auxiliary attributes rather than predefined class labels. Predictions are made by evaluating the similarity between image and text embeddings, derived from encoding both images and textual class descriptions [17]. Existing approaches like CLIP [21] tend to train image and text encoders to learn joint representations. Recent works [8, 23] have focused on improving zero-shot classification performance of CLIP by enhancing textual descriptions. In this work, we are the first to attain excellent zero-shot performance for DFA. Unlike CLIP which focuses solely on image-text matching, our BMRL method captures diverse global visual forgery features across image, noise, and edge perspectives, performing both vision-parsing matching and vision-language alignment to explore comprehensive and model-agnostic forensic representations.

## 3 Methodology

### 3.1 Problem Definition

For ZS-DFA, given a seen domain  $(X_s, Y_s)$  and an unseen domain  $(X_u, Y_u)$ , the input distributions of the seen and unseen domains are distinct, and there is no intersection between their label spaces, i.e.  $X_s \neq X_u$  and  $Y_s \cap Y_u = \emptyset$ , where  $X$  denotes the input distribution and  $Y$  represents the label space. ZS-DFA aims to learn a deepfake attributor, trained on the seen domain, to classify the distribution from the unseen domain. In our work, we employ the training set  $(I_s, y_s) \in \mathcal{D}_{tra}$  from the seen domain to train our model, and test it using the testing set  $(I_u, y_u) \in \mathcal{D}_{tes}$  from the unseen domain, where  $I$  denotes the input image,  $y \in \{e_i \mid e_i = (0, 0, \dots, 1, \dots, 0), 1 \leq i \leq$

$x\}$  denotes generator-specific one-hot labels,  $e_i \in \mathbb{R}^x$  represents the  $i$ -th one-hot label, and  $x$  is the number of generators.

### 3.2 Method Overview

To explore generalizable deepfake attribution patterns for ZS-DFA, we design the bi-modal guided multi-perspective representation learning (BMRL) model. As Figure 3 illustrates, our method mainly includes three key modules: multi-perspective visual encoder (MPVE), parsing encoder (PE), and language encoder (LE). During the training stage, given an input facial appearance image  $I^a$ , we leverage the Sobel operator [9], SRM [3], face parser [32], and fine-grained text generator [36] to obtain the edge image  $I^e$ , noise image  $I^n$ , parsing image  $P$ , and fine-grained attribution prompts  $T$ , respectively. Subsequently,  $I^a$ ,  $I^e$ , and  $I^n$  are fed into the MPVE to capture global visual attribution embeddings  $I_V$  across three perspectives. Meanwhile, BMRL transmits  $P$  and  $T$  to PE and LE, to extract the diverse global parsing features  $P_g$  and language attribution ones  $T_l$ , accordingly. Thereafter, we conduct the language-guided and parsing-guided deepfake attribution learning, respectively. We also conduct flexible metric learning, to focus on intra-generator compression as well as inter-generator separability, dynamically, to study general visual forgery features. Simultaneously, BMRL feds  $I_V$  to the predictor and MLP, both consisting of fully connected layers, to yield the predicted language embeddings  $T_l^{pre}$  and deepfake attribution ones, separately. Finally, we leverage the softmax function to yield the final prediction  $y_{pre}$ .

During the testing stage, BMRL utilizes MPVE to capture the visual deepfake attribution features across three perspectives, which are then transferred to the MLP head and softmax function, to produce the final prediction.

### 3.3 Multi-Perspective Visual Encoder

To capture comprehensive and general visual deepfake attribution embeddings, we propose the MPVE module to extract global multi-view features, since global representations are helpful for deepfake attribution as proven by [34]. Unlike existing multi-domain DFA methods [27, 29] which are inclined to focus on the interaction between the local frequency and RGB information, our MPVE module can dig appearance global forgery traces, fine-grained noise global representations, as well as edge global features, and integrate them to explore diverse and common global attribution embeddings across three views. As illustrated in Figure 3, MPVE mainly consists of an appearance encoder (AE), an edge encoder (EE), and a noise encoder (NE).

**Appearance encoder.** To extract global appearance deepfake attribution representations, we design AE, which consists of an appearance backbone with stacked convolutional layers followed by an appearance transformer encoder (ATE), following [31]. Particularly, given an input face appearance image  $I^a \in \mathbb{R}^{3 \times H \times W}$ , AE derives the locally manipulated feature map  $I_{loc}^a \in \mathbb{R}^{c \times h \times w}$  via the backbone, where  $H$  and  $W$  denote the height and width of the image, and  $c$ ,  $h$ ,  $w$  represent the channel, height, and width of the feature map, respectively. AE then sends it to the ATE block, to investigate global relationships among feature patches, to yield global appearance forgery embeddings  $I_g^a \in \mathbb{R}^{1 \times d}$ , where  $d$  denotes the dimension of the embeddings.

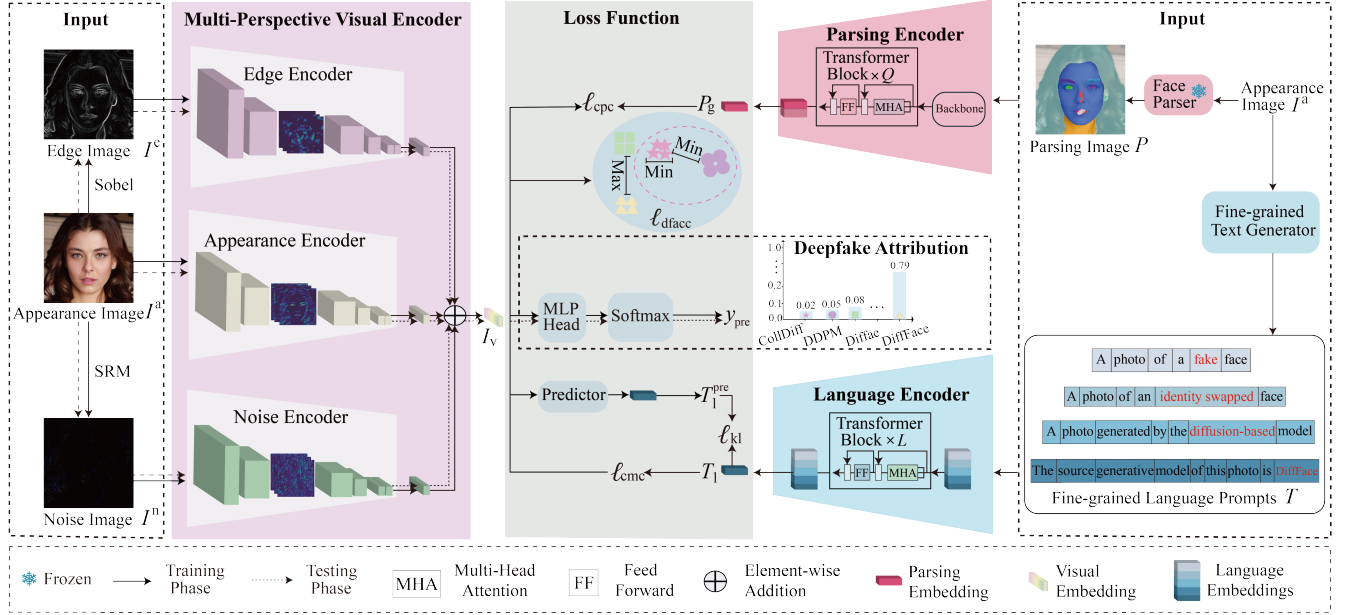


**Figure 3: The workflow of BMRL.** We first send the appearance image to the Sobel, SRM operator, face parser, and fine-grained text generator, to derive the edge image, noise image, parsing image, and text prompts, respectively. We then fed the appearance, edge, and noise image into MPVE to extract visual deepfake attribution features across multiple views. Meanwhile, the face parsing image and text prompts are transferred to the PE and LE to acquire face attribute features and language embeddings, accordingly. We then conduct the vision-parsing alignment, vision-language matching, and flexible metric learning. Finally, multi-view visual features are imparted to the MLP head and softmax to yield the prediction.

**Edge encoder.** To capture the comprehensive and diverse global relations among edge image patches, we devise the EE which contains an edge backbone with sequential convolutional layers and an edge transformer encoder with the same architecture as ATE. In detail, given the input facial appearance image  $I^a$ , we employ the Sobel operator [9] to acquire edge images  $I^e \in \mathbb{R}^{1 \times H \times W}$ . EE extracts the local edge forgery feature map  $I_{loc}^e \in \mathbb{R}^{c \times h \times w}$  via the backbone from  $I^e$ , which is then fed into the edge transformer encoder, to derive the global edge deepfake attribution embeddings  $I_g^e \in \mathbb{R}^{1 \times d}$ .

**Noise encoder.** To explore fine-grained discriminative and general noise attribution features, we propose the NE which is composed of a noise backbone with cascaded convolutional layers along with a noise transformer encoder with the same architecture as ATE. Specifically, given the input appearance image  $I^a$ , we extract the richest image patch via the patch selector in [36] from  $I^a$ , and then send them to the steganalysis rich model (SRM) [3] to gain the fine-grained discriminative noise image  $I^n \in \mathbb{R}^{3 \times p \times p}$ , where  $p$  denotes the height and width of the noise image. After that, like AE, NE encodes the local and global noise forgery representations to acquire  $I_g^n \in \mathbb{R}^{1 \times d}$ .

Finally, MPVE yields comprehensive and general visual deepfake attribution embeddings  $I_v$  by integrating  $I_g^a$ ,  $I_g^e$  with  $I_g^n$ , i.e.,  $I_v = I_g^a \oplus I_g^e \oplus I_g^n$ , which are then imparted to the predictor and the MLP head, respectively.  $\oplus$  denotes the element-wise addition.

### 3.4 Parsing Encoder

Different from current deepfake detection [29, 30, 35] or deepfake attribution methods [27, 28, 34] that tend to introduce discriminative

prior knowledge like identity, landmark, and frequency features, we focus on the face parsing information since the source face attributes in fake images tend to be incompletely preserved [19].

To further promote the model to study general deepfake attribution features, we design the parsing encoder (PE) consisting of a parsing backbone with stacked convolutional layers and a parsing transformer encoder (PTE) with  $Q$  transformer blocks,  $TB_j^P$ ,  $j = 1, 2, \dots, Q$ , to capture global face parsing representations. As shown in Figure 3, given the face appearance image, we leverage the CelebA-HQ pre-trained face parser [32] to generate the parsing image  $P \in \mathbb{R}^{3 \times H \times W}$ . Considering that the face parser may not accurately extract the parsing information of unseen faces, due to the domain gap between the pre-trained face dataset and the unseen one, we propose to conduct the parsing-guided multi-perspective DFA representation learning only during the training phase. Specifically, PE derives the local face parsing feature  $P_{loc} \in \mathbb{R}^{c \times h \times w}$  from  $P$  through the backbone, to conduct the feature alignment. PE then imparts it to PTE to explore diverse long-range relations among features. In detail,  $P_{loc}$  is appended with a learnable class token to capture the global parsing attribution features, to obtain  $P_{tok} = \text{App}(\text{Proj}(\text{Flat}(P_{loc}))) \in \mathbb{R}^{(n+1) \times d}$ , where  $n = \frac{chw}{chw}$  denotes the number of the parsing feature token sequence. It is then added with learnable position representations  $P_e \in \mathbb{R}^{(n+1) \times d}$  to encode the position information, i.e.,

$$P_1^{\text{tra}} = P_{\text{tok}} \oplus P_e. \quad (1)$$

Subsequently, it is consecutively fed into  $B$  blocks, i.e.,

$$\begin{aligned} \text{PTE}(p_1^{\text{tra}}) &= \text{TB}_B^{\text{p}} \circ \text{TB}_{B-1}^{\text{p}} \circ \dots \circ \text{TB}_2^{\text{p}} \circ \text{TB}_1^{\text{p}}(p_1^{\text{tra}}) \\ &= \text{TB}_B^{\text{p}} \circ \text{TB}_{B-1}^{\text{p}} \circ \dots \circ \text{TB}_2^{\text{p}}(p_2^{\text{tra}}) \\ &= \dots = \text{TB}_B^{\text{p}} \circ \text{TB}_{B-1}^{\text{p}}(p_{B-1}^{\text{tra}}) \\ &= \text{TB}_B^{\text{p}}(p_B^{\text{tra}}) = p_{\text{PTE}}^{\text{p}}, \end{aligned} \quad (2)$$

where  $\circ$  represents the function decomposition. PE derives global parsing attribution embeddings  $P_g \in \mathbb{R}^{1 \times d}$  using the class token in  $p_{\text{PTE}}^{\text{p}}$ . To perform parsing-aware multi-view visual representation learning, we achieve the vision-parsing matching via the proposed cross-perspective contrastive loss (See Sect. 3.6).

### 3.5 Language Encoder

To extract fine-grained deepfake attribution-aware language embeddings, we design the language encoder (LE). As Figure 3 illustrates, LE includes a language transformer encoder with  $L$  transformer blocks,  $\text{TB}_j^{\text{l}}$ ,  $j = 1, 2, \dots, L$ . In detail, given the fine-grained deepfake attribution prompts  $T$ , LE first yields a series of word tokens  $T^{\text{tok}} \in \mathbb{R}^t$  using the tokenizer [21], where  $t$  represents the number of word tokens. They are then projected to the word embedding vectors  $T^{\text{emb}} \in \mathbb{R}^{t \times d}$ , and added with learnable position embeddings  $P_l \in \mathbb{R}^{t \times d}$ , i.e.,  $T_1^{\text{tra}} = T^{\text{emb}} \oplus P_l$ . Thereafter, they are consecutively transferred to  $L$  blocks, to derive the language attribution features  $T_{\text{LE}}^1 \in \mathbb{R}^{t \times d}$ . LE obtains the global deepfake attribution-perceptual language representations  $T_l \in \mathbb{R}^{1 \times d}$  using the class token in  $T_{\text{LE}}^1$ , which are then used for vision-language matching (See Sect. 3.6).

### 3.6 Loss Function

**Deepfake attribution loss.** To capture discriminative deepfake attribution representations, we introduce the DFA loss. Specifically, the visual forgery patterns across three perspectives  $I_v$  are fed into the MLP head with a fully connected layer followed by a softmax function, to produce the final prediction  $y_{\text{pre}} \in \mathbb{R}^x$ . The DFA loss is defined as follows:

$$\mathcal{L}_{\text{dfa}} = \frac{1}{b} \sum_{u=1}^b -(y^u)^T \log(y_{\text{pre}}^u), \quad (3)$$

where  $x$  is the number of the deepfake generators,  $b$  denotes the number of samples in a batch, and  $u \in b$  is the index of samples.

**Deepfake attribution contrastive center loss.** However, learned deepfake attribution features are not general enough since the DFA loss merely considers the decision boundary among generators, rather than intra-generator compression as well as inter-generator separability, flexibly. To address the limitation, we propose an innovative deepfake attribution contrastive center (DFACC) loss. Unlike vanilla contrastive center loss [20] applied for ZS-DFA tasks which makes intra-generator samples closer and inter-generator ones farther apart, our DFACC loss minimizes the distance among within-generator samples, while places correlated samples across generators closer and uncorrelated ones stay away from each other. In detail, the proposed DFACC criterion is defined as  $\mathcal{L}_{\text{dfacc}} = \mathcal{L}_{\text{intra}} + \lambda \mathcal{L}_{\text{inter}}$ . To achieve the intra-generator compaction, we design the  $\mathcal{L}_{\text{intra}}$  loss as follows:

$$\mathcal{L}_{\text{intra}} = \frac{1}{b} \sum_{u=1}^b \|y_{\text{pre}}^u - c_{y^u}\|_2, \quad (4)$$

where  $c_{y^u} \in \mathbb{R}^d$  denotes the trainable center vector of the generator  $y^u$ ,  $\|\cdot\|_2$  is the Euclidean distance,  $\lambda$  is the factor to balance the loss term, and  $y^u$  denotes the generator-specific one-hot label of the sample  $u$ .

To minimize the distance among relevant samples across generators, and maximize the distance among unrelated ones, we propose the  $\mathcal{L}_{\text{inter}}$  loss,

$$\mathcal{L}_{\text{inter}} = \frac{2}{b(b-1)} \sum_{u=1}^b \sum_{v=u+1}^b \mathbb{I}(y^u \neq y^v) \cdot \mathcal{L}_{uv}, \quad (5)$$

$$\mathbb{I}(y^u \neq y^v) = \begin{cases} 1, & \text{if } y^u \neq y^v, \\ 0, & \text{if } y^u = y^v, \end{cases} \quad (6)$$

$$\mathcal{L}_{uv} = \begin{cases} \max(\|y_{\text{pre}}^u - y_{\text{pre}}^v\|_2 - m, 0) & \text{if } \|c_{y^u} - c_{y^v}\|_2 < m, \\ -\|y_{\text{pre}}^u - y_{\text{pre}}^v\|_2 & \text{if } \|c_{y^u} - c_{y^v}\|_2 \geq m, \end{cases} \quad (7)$$

where  $m$  is a predefined margin threshold, to control the interval among samples,  $\mathbb{I}$  is the indicator function, and  $u, v = 1, 2, \dots, b$  is the sample index.

**Cross-modal contrastive loss.** To perform vision-language matching, we introduce the cross-modal contrastive (CMC) loss, to enhance the visual deepfake attribution embeddings. The detailed workflow of the CMC loss  $\mathcal{L}_{\text{cmc}}$  is discussed in [36].

**Kullback-leibler divergence loss.** To further conduct the feature alignment, we introduce the kullback-leibler (KL) divergence loss. In detail, we transfer visual embeddings  $I_v$  to a predictor with a full connection layer, to yield the predicted language representations  $T_1^{\text{pre}} \in \mathbb{R}^{1 \times d}$ . Like [36], we employ the KL divergence loss  $\mathcal{L}_{\text{kl}}$  to narrow the distance between  $T_1^{\text{pre}}$  and  $T_l$ .

**Cross-perspective contrastive loss.** To achieve the vision-parsing contrastive learning, inspired by vision-language matching, we devise the cross-perspective contrastive (CPC) loss, to conduct the parsing-guided visual deepfake attribution learning. Mathematically, for the vision-parsing feature pairs  $\{(I_v^u, P_g^u)\}_{u=1}^b$ , we calculate the vision-parsing cosine similarity vector and the parsing-vision one as follows:

$$S_{v2p}^{uv}(I_v, P_g) = \frac{\exp(\text{sim}(I_v^u, P_g^u)/\tau)}{\sum_{v=1}^b \exp(\text{sim}(I_v^u, P_g^u)/\tau)}, \quad (8)$$

$$S_{p2v}^{uv}(P_g, I_v) = \frac{\exp(\text{sim}(P_g^u, I_v^u)/\tau)}{\sum_{v=1}^b \exp(\text{sim}(P_g^u, I_v^u)/\tau)}, \quad (9)$$

where  $\tau$  is a learnable temperature parameter initialized with 0.07, to smooth embeddings, the function  $\text{sim}(\cdot)$  executes a dot product operation to compute the similarity scores, and  $u, v = 1, 2, \dots, b$  are the index of the sample. The one-hot label  $y_{\text{pa}}$  of the  $u$ -th pair is denoted as  $y_{\text{pa}}^u = \{y_{\text{pa}}^{uv}\}_{v=1}^b$ ,  $y_{\text{pa}}^{uu} = 1$ ,  $y_{\text{pa}}^{uv, u \neq v} = 0$ . To pull positive pairs together, while pushing negative ones away, the CPC loss

function is denoted as  $\mathcal{L}_{\text{cpc}} = (\mathcal{L}_{v2p} + \mathcal{L}_{p2v})/2$ , where

$$\mathcal{L}_{v2p} = \frac{1}{b} \sum_{u=1}^b -(y_{pa}^u)^T \log(S_{v2p}^u), \quad (10)$$

$$\mathcal{L}_{p2v} = \frac{1}{b} \sum_{u=1}^b -(y_{pa}^u)^T \log(S_{p2v}^u). \quad (11)$$

The total loss is defined as follows:

$$\mathcal{L}_{\text{total}} = \mathcal{L}_{\text{dfa}} + \mathcal{L}_{\text{dfacc}} + \mathcal{L}_{\text{cmc}} + \mathcal{L}_{\text{cpc}} + \mathcal{L}_{\text{kl}}. \quad (12)$$

## 4 Experiments

### 4.1 Experiment Setup

**Dataset collection and protocol.** We collect real and fake face images created by various advanced generators, including GAN and diffusion based on several datasets, such as GenFace [37], DF40 [33], CelebAHQ [10], and FFHQ [12]. As Table 2 shows, these fake data mainly involve three manipulations, including entire face synthesis (EFS), attribute manipulation (AM), and face swap (FS). Each forgery contains GAN-based or diffusion-based generators. As Table 2 displays, we define two protocols to evaluate the attribution performance of various models under zero-shot scenarios: 1) **Protocol-1** intends to investigate the performance of different attributors on unseen generators. It consists of 19 generators such as GAN-based and diffusion-based ones from both the GenFace and DF40 Dataset. We also generate the 2k fake faces using the CelebA-HQ pre-trained REFace model [1], which is a diffusion-based FS method. 2) **Protocol-2** introduces additional real faces from both CelebA-HQ and FFHQ datasets based upon protocol-1, considering that real faces may appear on social media platforms.

**Evaluation metrics.** We leverage accuracy (ACC) as our evaluation metrics. For zero-shot settings, we obtain the maximum probability from logits yielded by the softmax function. We define a threshold to evaluate whether the model has encountered the generator or not. Specifically, we label the generator as unseen, when the maximum probability falls below the threshold. We set the threshold to 0.7 and 0.9, respectively, and only report the results for the threshold of 0.9 on protocol-1 in the ablation study.

**Implementation details.** We implement the model using PyTorch on a Tesla V100 GPU with 32GB memory. The number of transformer blocks  $Q$  and  $L$  in BMRL are set to 6. The patch size  $p$ , feature dimension  $d$ , the factor  $\lambda$ , and batch size  $b$  are set to 112, 512, 0.5, and 32, respectively. We set the channel  $c$ , height  $h$ , and width  $w$  of feature maps to 512, 7, and 7, accordingly. The height  $H$  and width  $W$  of images are configured to 224. We set the number  $t$  of word tokens to 308. Our method is trained with the Adam optimizer [15] using a learning rate of  $1e-4$  and a weight decay of  $1e-3$ . We leverage the scheduler to drop the learning rate by ten times every 15 epochs. We conduct the normalization by dividing the image pixel values by 255, without any data augmentation operations. To ensure a fair comparison, we develop the SOTA methods using codes provided by authors and follow the default configurations, until convergence. All models are trained and evaluated using the same dataset protocols.

### 4.2 Comparison with the State of the Art

**Results on protocol-1.** To study the ZS-DFA performance of different models, we conduct the cross-generator evaluation on protocol-1. We test models on various unseen generators from DF40 after training using seen generators from GenFace. As Table 1 shows, our method exceeds most attributors by a wide gap. It also surpasses the recent network, MFCLIP, by about 12% ACC under the threshold of 0.7. Unlike MFCLIP which conducts the fine-grained language-guided image-noise forgery representation learning, our model introduces face parsing global features, and performs the bi-modality (e.g., text and parsing) guided multiple perspectives (e.g., image, noise, and edge) deepfake attribution representation learning. Compared to the DFA methods, the ACC of our method is nearly 4%, 12%, and 17% higher than that of CPL, DNA-Det, and DE-FAKE, validating the effectiveness of our model. Different from DNA-Det which only explores global attribution representations within the image modality via patch-based contrastive learning, our approach focuses on multiple modalities including text and face parsing, and multiple perspectives such as image, noise, and edge forgery embeddings, to achieve predominant ZS-DFA performance.

**Results on protocol-2.** To further assess the attribution performance of various methods, we conduct the ZS-DFA evaluation on protocol-2. We test models on various unseen generators and FFHQ after training using both seen generators and CelebA-HQ. As Table 3 displays, the ACC of our method exceeds that of most SOTAs, showing the superior ZS-DFA capability of the proposed attributor. Specifically, the average ACC score of our BMRL model is about 18.56% higher than that of CViT on protocol-2. Unlike CViT merely explores global image forgery traces, our method focuses on global visual forgery features across three views (i.e., image, noise, and edge) and conducts fine-grained vision-language alignment and vision-parsing matching. Besides, models trained using protocol-2 outperform those trained with protocol-1. For instance, CAEL, MFCLIP, and DNA-Det gain the average ACC score of 21.46%, 38.70%, and 32.63% under the threshold of 0.9 setting on protocol-1, respectively. By contrast, they attain 30.86% ACC, 43.38% ACC and 50.48% ACC on protocol-2, accordingly. It is noticed that a nearly 9.4%, 4.7%, and 17.85% growth of ACC could be realized by introducing real face distributions, which indicates that pristine face images could facilitate the ZS-DFA performance of various deepfake attributors. We argue that models may extract more discriminative and comprehensive forgery embeddings for each generator, due to the introduction of authentic face distributions, thus boosting the learning of general deepfake attribution representations.

**Robustness to unseen image corruptions.** We evaluate the robustness of deepfake attributors against various unseen image perturbations. We train networks using the protocol-1, and test their ZS-DFA performance on unseen distorted images from [7]. Seven types of corruptions are engaged, each with five severity levels. As Figure 4 displays, we test attributors on diverse image distortions, including saturation changes, contrast adjustments, block distortions, white Gaussian noise, blurring, pixelation, and video compression. An severity of 0 means no corruptions. Specifically, the specific settings for the severity of the seven deformations are discussed in detail in [37]. In Figure 4, models consistently exhibit

**Table 1: ZS-DFA evaluation on protocol-1. ACC scores (%) on unseen generators, after training using seen generators. Bold and underline denote the best and the second-best results.**

Methods	SimSwap		InSwapper		UniFace		e4s		VQGAN		SD-2.1		DiT		SiT		REFace		Average	
	Thr 0.7	Thr 0.9																		
CLIP [21]	9.12	17.44	<u>20.16</u>	28.08	18.24	28.56	<b>37.60</b>	<u>59.52</u>	7.20	10.72	19.52	36.32	10.48	17.76	14.40	23.28	<b>64.88</b>	<b>77.76</b>	22.40	33.27
CViT [31]	11.76	25.04	8.08	20.08	13.44	27.04	26.72	48.00	25.76	47.04	15.84	34.08	21.52	39.52	20.24	37.44	15.04	31.92	17.60	34.46
CAEL [37]	3.36	6.56	5.04	9.52	5.44	9.60	20.48	43.04	0.80	1.92	<b>36.56</b>	<b>61.44</b>	1.92	5.44	2.64	6.56	23.28	49.12	11.06	21.46
MFCLIP [36]	21.36	46.72	13.76	31.12	20.40	44.96	29.76	57.04	14.88	35.76	12.72	26.16	13.52	30.16	10.64	27.12	25.92	49.28	18.11	38.70
DNA-Det [34]	6.04	16.72	4.20	10.2	3.04	10.16	28.76	59.28	<u>29.08</u>	58.64	11.52	27.20	25.32	49.96	21.88	44.12	33.20	62.36	18.12	32.63
CPL [28]	<u>22.81</u>	<u>67.90</u>	14.54	<u>42.60</u>	<u>22.67</u>	<u>56.82</u>	<u>30.48</u>	<b>60.04</b>	<b>30.80</b>	<u>61.92</u>	13.74	38.44	<u>26.92</u>	<u>65.40</u>	<u>22.70</u>	<u>66.82</u>	35.28	63.12	<u>26.68</u>	<u>58.12</u>
CARZero [16]	2.21	3.82	2.07	3.73	2.43	3.71	9.36	17.04	3.61	6.92	7.91	17.44	2.03	3.59	3.01	5.37	9.36	20.05	4.67	9.07
DE-FAKE [25]	0.48	1.36	0.48	1.52	0.96	2.64	7.12	15.36	2.00	5.52	6.96	15.76	0.72	2.24	1.28	3.04	8.24	19.44	3.14	7.43
BMRL (Ours)	<b>26.16</b>	<b>69.36</b>	<b>43.92</b>	<b>84.96</b>	<b>26.88</b>	<b>66.32</b>	10.63	35.60	26.80	<b>67.60</b>	<u>22.64</u>	<u>46.16</u>	<b>40.56</b>	<b>81.20</b>	<b>40.08</b>	<b>81.68</b>	<u>38.08</u>	<u>63.92</u>	<b>30.64</b>	<b>66.31</b>

**Table 2: The outline of the dataset construction and protocol. # denotes the number of dataset. Pro means the protocol.**

Seen Sets	Unseen Sets	Type	Sub-Type	Generator	Train #	Test #	Pro-1	Pro-2
GenFace	-	EFS	GAN	StyleGAN2	10,000	1,250	✓	✓
GenFace	-	EFS	GAN	StyleGAN3	10,000	1,250	✓	✓
GenFace	-	EFS	Diffusion	LatDiff	10,000	1,250	✓	✓
GenFace	-	EFS	Diffusion	CollDiff	10,000	1,250	✓	✓
GenFace	-	EFS	Diffusion	DDPM	10,000	1,250	✓	✓
GenFace	-	FS	GAN	FSLSD	10,000	1,250	✓	✓
GenFace	-	FS	GAN	FaceSwapper	10,000	1,250	✓	✓
GenFace	-	FS	Diffusion	DiffFace	10,000	1,250	✓	✓
GenFace	-	AM	GAN	LatTrans	10,000	1,250	✓	✓
GenFace	-	AM	Diffusion	Diffae	10,000	1,250	✓	✓
-	DF40	EFS	GAN	VQGAN	-	1,250	✓	✓
-	DF40	EFS	Diffusion	SD-2.1	-	1,250	✓	✓
-	DF40	EFS	Diffusion	DiT	-	1,250	✓	✓
-	DF40	FS	GAN	SimSwap	-	1,250	✓	✓
-	DF40	FS	GAN	UniFace	-	1,250	✓	✓
-	DF40	FS	GAN	InSwapper	-	1,250	✓	✓
-	DF40	FS	GAN	e4s	-	1,250	✓	✓
-	DF40	FS	Diffusion	REFace	-	1,250	✓	✓
CelebAHQ	-	Real	-	-	10,000	1,250	×	×

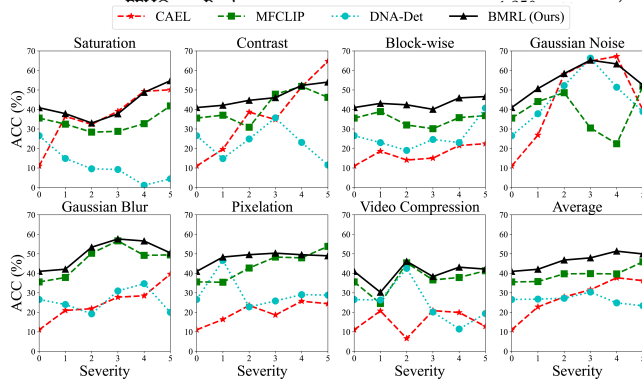


**Figure 4: Robustness to unknown image deformations.**

sensitivity to deformations such as Gaussian noise. Besides, our attributor outperforms most networks across different types of image perturbations.

### 4.3 Ablation Study

**Effects of various modules.** To evaluate the contribution of each module to learning ability, we observe the deepfake attribution performance on both seen and unseen generators under protocol 1. Table 6 presents the ablation results of networks. NE improves the performance of the attributor by 2.34% ACC on images created by unseen generators, showing that SRM noises provide significant clues to facilitate ZS-DFA. The improvement from incorporating the

EE components (+2.48%) are clear, highlighting the importance of edge global embeddings. LE further boosts performance by 21.97% ACC, indicating that ZS-DFA can gain from fine-grained deepfake attribution language representations. The introduction of PE increases the performance by 5.06% in accuracy, demonstrating that face parsing features can equip useful information to guide the model to extract general deepfake attribution clues.

**Impacts of the DFACC loss.** To verify the contribution of the proposed DFACC loss, models are trained with the vanilla contrastive center loss and the DFACC loss, respectively. As Table 4 shows, the ACC of both CLIP and BMRL supervised by the VCC loss are 79.04% and 96.85% on protocol-1, respectively. By contrast, they achieve 79.04% ACC and 96.85% ACC under the constriction of our DFACC criteria, accordingly, which verifies the necessity of conducting intra-generator compactness and inter-generator separability based on the correlation among generators, flexibly.

**Influences of the face parser.** We delve into the impact of various face parsers, such as SegFace [18] and BiSeNet [32]. We test frameworks on protocol-1. The ablation results are displayed in Table 5. The ACC reaches the maximum as the BiSeNet is involved. We argue that face parsing features extracted by BiSeNet are more discriminative than those encoded by other face parsers, which could boost the deepfake attribution performance.

## 5 Visualization

**Visualization of heatmaps.** To enhance the interpretability of the proposed method, we visualize the heatmap yielded by various settings using the Grad-CAM [24]. In Figure 5, we show the heatmap of samples generated by various seen and unseen generators for three models, respectively. Each column shows a fake face synthesized by different generators. The second to fourth rows display heatmaps for three models listed in Table 1: DNA-Det, MFCLIP, and our BMRL method. It is observed that BMRL mines more comprehensive forgery traces than both MFCLIP and DNA-Det. As shown in Figure 5, attributors tend to identify forgery regions such as eyes, nose and mouth. It is noted that DFA could be regarded as a fine-grained forgery detection task, since manipulated artifacts created by generators are prone to be subtle and faint.

**Visualization of T-SNE.** To study the impact of the proposed DFACC loss on feature distributions, we visualize features extracted from samples produced by various generators using t-SNE. As is illustrated in Figure 6, features of each generator are clustered in respective domains. With the addition of the DFACC loss, sample features within the generator are more compact, with those of

**Table 3: ZS-DFA evaluation on protocol-2. ACC scores (%) on unseen generators and FFHQ, after training using seen generators and CelebA-HQ. Bold and underline denote the best and the second-best results.**

Methods	SimSwap		InSwapper		UniFace		e4s		VQGAN		SD-2.1		DiT		SiT		REFace		FFHQ		Average	
	Thr 0.7	Thr 0.9																				
CLIP [21]	16.80	21.92	19.12	27.04	14.88	21.20	<b>40.56</b>	62.80	12.16	15.36	24.64	42.24	14.08	18.72	15.92	23.04	<b>86.80</b>	<b>88.64</b>	<b>25.84</b>	<b>38.80</b>	27.08	35.98
CViT [31]	28.24	49.04	19.44	39.04	29.84	50.00	21.20	37.04	16.16	31.52	17.60	42.40	22.24	45.68	<u>22.96</u>	<u>46.56</u>	3.36	8.32	2.56	7.52	18.36	35.71
CAEL [37]	4.88	12.24	8.96	21.6	6.96	18.00	33.12	<u>65.36</u>	18.40	36.64	<b>31.92</b>	<b>64.80</b>	3.52	8.08	4.48	9.60	30.40	62.08	3.92	10.16	14.66	30.86
MFCLIP [36]	33.68	63.20	35.28	64.16	34.08	63.84	24.96	50.48	<u>34.72</u>	63.12	11.76	25.84	22.00	39.28	18.88	33.84	10.48	28.32	0.88	1.76	22.67	43.38
DNA-Det [34]	27.56	61.60	26.28	63.84	18.20	50.16	<u>39.48</u>	<b>77.56</b>	26.32	50.00	19.84	34.08	16.68	39.32	13.20	33.16	42.32	79.16	7.96	15.96	23.78	50.48
CPL [28]	<u>35.70</u>	<u>68.38</u>	<u>37.03</u>	<u>75.77</u>	<u>36.26</u>	<u>75.49</u>	28.55	62.06	<b>35.69</b>	<b>74.58</b>	12.65	37.99	<u>24.87</u>	<u>51.53</u>	20.21	45.60	42.72	<u>80.51</u>	8.90	16.64	<u>28.26</u>	<u>58.86</u>
CARZero [16]	3.04	4.90	2.76	3.49	2.54	3.09	10.43	20.44	3.73	7.21	6.19	14.03	1.36	3.45	2.88	5.25	9.37	19.02	13.47	25.01	6.20	11.72
DE-FAKE [25]	1.12	2.32	1.36	2.88	1.20	2.48	8.56	19.84	2.40	5.12	5.92	13.28	0.80	1.92	1.60	3.52	6.48	17.44	11.68	24.24	4.11	9.30
BMRL (Ours)	<b>36.60</b>	<b>71.12</b>	<b>53.76</b>	<b>86.90</b>	<b>38.96</b>	<u>71.68</u>	15.76	39.36	33.36	<u>73.44</u>	<u>30.47</u>	<u>48.70</u>	<b>50.23</b>	<b>84.76</b>	<b>50.38</b>	<b>88.02</b>	<u>44.90</u>	78.90	<u>14.73</u>	<u>26.05</u>	<b>36.92</b>	<b>66.89</b>

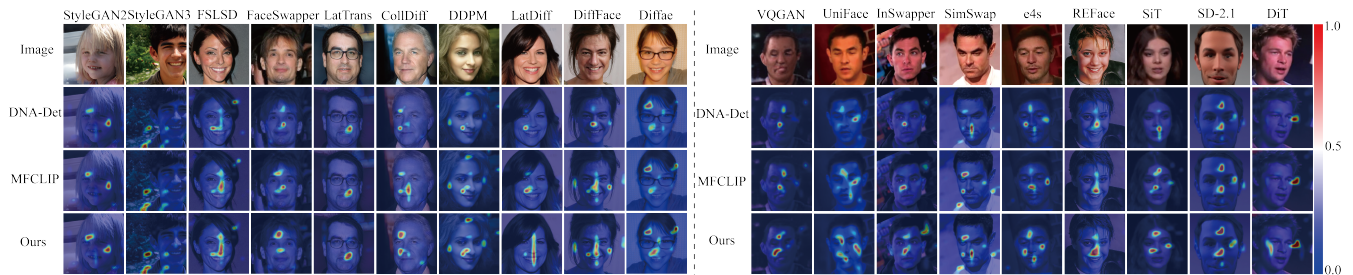


**Figure 5: The heatmap visualization of various models on the sample created by the seen (Left) or unseen (Right) generators.**

**Table 4: Effects of various losses. VCC is the vanilla contrastive center loss.**

Method	Protocol-1	
	Seen	Unseen
	ACC	ACC
CLIP w/VCC	79.04	-
CLIP w/DFACC	89.07	-
Ours w/VCC	96.85	62.47
Ours w/DFACC	<b>100</b>	<b>66.31</b>

**Table 5: Effects of various face parsers.**

Method	Protocol-1	
	Seen	Unseen
	ACC	ACC
SegFace w/ConNet [18]	95.32	46.34
SegFace w/ResNet [18]	97.54	58.50
SegFace w/ Swin-B [18]	96.87	47.38
BiSeNet [32]	<b>100</b>	<b>66.31</b>

**Table 6: Model ablation. ACC scores (%) on Protocol-1.**

Model					Seen	Unseen
AE	NE	EE	PE	LE	ACC	ACC
✓					99.58	34.46
		✓			99.83	29.71
	✓				99.66	23.97
✓	✓				99.72	36.80
✓	✓			✓	100	38.70
✓	✓			✓	100	61.64
✓		✓			99.99	34.62
✓	✓	✓			99.76	39.28
✓	✓	✓		✓	100	61.25
✓	✓	✓	✓	✓	100	66.31

highly correlated generators aggregated and those of weakly related ones separated. Specifically, samples created by generators under the EFS forgery including StyleGAN3 [11], StyleGAN2 [13], CollDiff [6], and LatDiff [22] are inclined to cluster in the feature space, where those of the generator with strong relevance (i.e., StyleGAN2 and StyleGAN3) are more closely gathered. This shows that our DFACC loss achieves flexible intra-generator aggregation and inter-generator separation.

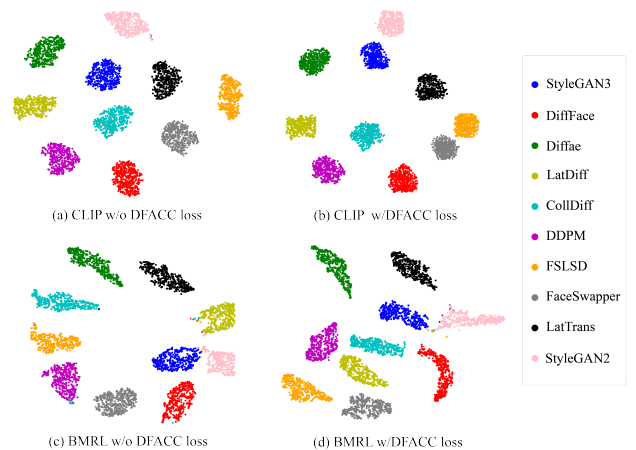


**Figure 6: The t-SNE visualization of different models (w/o or w/ DFACC loss). We randomly select 500 samples for each seen generator from the testing dataset of protocol-1.**

## 6 Deepfake Detection

To demonstrate the significance of deepfake attribution, we evaluate the performance of the deepfake detection and attribution model using Protocol-2. The results of models on two tasks (i.e., deepfake detection and deepfake attribution) are displayed in Table 7. It is noticed that the classification tends to become easier, with the number of categories increasing from 2 (deepfake detection) to 11 (deepfake attribution). We argue that there is a growing distinction between pristine and forged images, as the number of categories rises, which facilitates deepfake detection. For example, MFCLIP and DNA-Det obtain 99.74% ACC and 96.18% ACC on seen generators under the deepfake detection setting, respectively. By contrast, they achieve

**Table 7: ACC results (%) of models for deepfake detection and deepfake attribution on protocol-2.**

Method	Deepfake Detection		Deepfake Attribution	
	Seen	Unseen	Seen	Unseen
	ACC	ACC	ACC	ACC
CLIP [21]	73.56	63.08	82.72	35.98
CAEL [37]	99.63	83.09	99.83	30.86
MFCLIP [36]	99.74	86.49	99.91	43.38
DE-FAKE [25]	97.07	69.32	98.15	9.30
DNA-Det [34]	96.18	67.02	99.65	50.48
BMRL (Ours)	<b>99.86</b>	<b>88.32</b>	<b>100</b>	<b>66.89</b>

99.91% ACC (+0.17%) and 99.65% ACC (+2.47%) on seen generators in deepfake attribution tasks, accordingly.

## 7 Conclusion

In this paper, we design a novel BMRL method for ZS-DFA. First, we devise the multi-perspective visual encoder to capture general and comprehensive visual deepfake attribution embeddings across three views (i.e., image, edge, and noise). Second, we observe that there are evident distinctions between the real, GAN, and diffusion face parsing images. We propose the parsing encoder to extract the discriminative attribution features. We also build the language encoder to encode rich and fine-grained DFA language embeddings. Finally, we present the deepfake attribution contrastive center loss to achieve flexible metric learning.

**Limitations.** Although our method has explored comprehensive and general deepfake attribution representations, we need to consider more diverse and advanced generators. In the future, we plan to introduce abundant face data generated by various generators like flow-based and auto-regressive models, to facilitate ZS-DFA.

## References

- [1] Sanooran Baliah, Qinliang Lin, Shengcai Liao, Xiaodan Liang, and Muhammad Haris Khan. 2025. Realistic and Efficient Face Swapping: A Unified Approach with Diffusion Models. In *Proceedings of the Winter Conference on Applications of Computer Vision (WACV)*. 1062–1071.
- [2] Harry Cheng, Yangyang Guo, Tianyi Wang, Liqiang Nie, and Mohan Kankanhalli. 2024. Diffusion Facial Forgery Detection. In *Proceedings of the 32nd ACM International Conference on Multimedia (MM)*. 5939–5948.
- [3] Jessica Fridrich and Jan Kodovsky. 2012. Rich models for steganalysis of digital images. *IEEE Transactions on Information Forensics and Security* 7, 3 (2012), 868–882.
- [4] Sharath Girish, Saksham Suri, Sai Saketh Rambhatla, and Abhinav Shrivastava. 2021. Towards discovery and attribution of open-world gan generated images. In *Proceedings of the IEEE international conference on computer vision (CVPR)*. 14094–14103.
- [5] Ian Goodfellow, Jean Pouget-Abadie, Mehdi Mirza, Bing Xu, David Warde-Farley, Sherjil Ozair, Aaron Courville, and Yoshua Bengio. 2014. Generative Adversarial Nets. In *Proceedings of the Advances in Neural Information Processing Systems (NIPS)*. 2672–2680.
- [6] Ziqi Huang, Kelvin CK Chan, Yuming Jiang, and Ziwei Liu. 2023. Collaborative diffusion for multi-modal face generation and editing. In *Proceedings of the IEEE Conference on Computer Vision and Pattern Recognition (CVPR)*. 6080–6090.
- [7] Liming Jiang, Ren Li, Wayne Wu, Chen Qian, and Chen Change Loy. 2020. DeeperForensics-1.0: A Large-Scale Dataset for Real-World Face Forgery Detection. In *Proceedings of the IEEE Conference on Computer Vision and Pattern Recognition (CVPR)*. 2886–2895.
- [8] Yannis Kalantidis, Giorgos Tolias, et al. 2024. Label propagation for zero-shot classification with vision-language models. In *Proceedings of the IEEE Conference on Computer Vision and Pattern Recognition (CVPR)*. 23209–23218.
- [9] Nick Kanopoulos, Nagesh Vasanthavada, and Robert L Baker. 1988. Design of an image edge detection filter using the Sobel operator. *IEEE Journal of Solid-state Circuits* 23, 2 (1988), 358–367.
- [10] Tero Karras, Timo Aila, Samuli Laine, and Jaakko Lehtinen. 2018. Progressive Growing of GANs for Improved Quality, Stability, and Variation. In *Proceedings of the International Conference on Learning Representations (ICLR)*. 26–37.
- [11] Tero Karras, Miika Aittala, Samuli Laine, Erik Härkönen, Janne Hellsten, Jaakko Lehtinen, and Timo Aila. 2021. Alias-Free Generative Adversarial Networks. In *Proceedings of the Neural Information Processing Systems (NIPS)*. 852–863.
- [12] Tero Karras, Samuli Laine, and Timo Aila. 2019. A Style-Based Generator Architecture for Generative Adversarial Networks. In *Proceedings of the IEEE Conference on Computer Vision and Pattern Recognition (CVPR)*. 4396–4405.
- [13] Tero Karras, Samuli Laine, Miika Aittala, Janne Hellsten, Jaakko Lehtinen, and Timo Aila. 2020. Analyzing and Improving the Image Quality of StyleGAN. In *Proceedings of the IEEE Conference on Computer Vision and Pattern Recognition (CVPR)*. 8107–8116.
- [14] Kihong Kim, Yunho Kim, Seokju Cho, Junyoung Seo, Jisu Nam, Kychul Lee, Seungryong Kim, and KwangHee Lee. 2022. DiffFace: Diffusion-based face swapping with facial guidance. *arXiv preprint arXiv:2212.13344* (2022).
- [15] Diederik P. Kingma and Jimmy Ba. 2015. Adam: A Method for Stochastic Optimization. In *Proceedings of the International Conference on Learning Representations (ICLR)*. 1–15.
- [16] Haoran Lai, Qingsong Yao, Zihang Jiang, Rongsheng Wang, Zhiyang He, Xiaodong Tao, and S. Kevin Zhou. 2024. CARZero: Cross-Attention Alignment for Radiology Zero-Shot Classification. In *Proceedings of the IEEE Conference on Computer Vision and Pattern Recognition (CVPR)*. 11137–11146.
- [17] Yudong Li, Xianxu Hou, Zheng Dezhi, Linlin Shen, and Zhe Zhao. 2024. FLIP-80M: 80 Million Visual-Linguistic Pairs for Facial Language-Image Pre-Training. In *Proceedings of the ACM International Conference on Multimedia (MM)*. 58–67.
- [18] Kartik Narayan, Vibashan VS, and Vishal M Patel. 2024. Segface: Face segmentation of long-tail classes. *arXiv preprint arXiv:2412.08647* (2024).
- [19] Gan Pei, Jiangning Zhang, Menghan Hu, Zhenyu Zhang, Chengjie Wang, Yunsheng Wu, Guangtao Zhai, Jian Yang, Chunhua Shen, and Dacheng Tao. 2024. Deepfake generation and detection: A benchmark and survey. *arXiv preprint arXiv:2403.17881* (2024).
- [20] Ce Qi and Fei Su. 2017. Contrastive-center loss for deep neural networks. In *Proceedings of the IEEE International Conference on Image Processing (ICIP)*. 2851–2855.
- [21] Alec Radford, Jong Wook Kim, Chris Hallacy, Aditya Ramesh, Gabriel Goh, Sandhini Agarwal, Girish Sastry, Amanda Askell, Pamela Mishkin, Jack Clark, et al. 2021. Learning transferable visual models from natural language supervision. In *Proceedings of the International Conference on Machine Learning (ICML)*. 8748–8763.
- [22] Robin Rombach, Andreas Blattmann, Dominik Lorenz, Patrick Esser, and Björn Ommer. 2023. High-resolution image synthesis with latent diffusion models. In *Proceedings of the IEEE Conference on Computer Vision and Pattern Recognition (CVPR)*. 10684–10695.
- [23] Oindrila Saha, Grant Van Horn, and Subhransu Maji. 2024. Improved zero-shot classification by adapting vlms with text descriptions. In *Proceedings of the IEEE Conference on Computer Vision and Pattern Recognition (CVPR)*. 17542–17552.
- [24] Ramprasaath R. Selvaraju, Michael Cogswell, Abhishek Das, Ramakrishna Vedantam, Devi Parikh, and Dhruv Batra. 2017. Grad-CAM: Visual Explanations from Deep Networks via Gradient-Based Localization. In *Proceedings of the IEEE International Conference on Computer Vision (ICCV)*. 618–626.
- [25] Zeyang Sha, Zheng Li, Ning Yu, and Yang Zhang. 2023. DE-FAKE: Detection and Attribution of Fake Images Generated by Text-to-Image Generation Models. In *Proceedings of the ACM SIGSAC Conference on Computer and Communications Security*. 3418–3432.
- [26] Jordan Shipard, Arnold Wiliem, Kien Nguyen Thanh, Wei Xiang, and Clinton Fookes. 2023. Diversity is definitely needed: Improving model-agnostic zero-shot classification via stable diffusion. In *Proceedings of the IEEE Conference on Computer Vision and Pattern Recognition (CVPR)*. 769–778.
- [27] Zhimin Sun, Shen Chen, Taiping Yao, Ran Yi, Shouhong Ding, and Lizhuang Ma. 2024. Rethinking Open-World DeepFake Attribution with Multi-perspective Sensory Learning. *Int. J. Comput. Vision* 133, 2 (Aug. 2024), 628–651.
- [28] Zhimin Sun, Shen Chen, Taiping Yao, Bangjie Yin, Ran Yi, Shouhong Ding, and Lizhuang Ma. 2023. Contrastive Pseudo Learning for Open-World DeepFake Attribution. In *Proceedings of the IEEE International Conference on Computer Vision (ICCV)*. 20825–20835.
- [29] Chuangchuang Tan, Yao Zhao, Shikui Wei, Guanghua Gu, Ping Liu, and Yunchao Wei. 2024. Frequency-Aware Deepfake Detection: Improving Generalizability through Frequency Space Domain Learning. In *Proceedings of the AAAI Conference on Artificial Intelligence (AAAI)*, Vol. 38. 5052–5060.
- [30] Tianyi Wang, Mengxiao Huang, Harry Cheng, Xiao Zhang, and Zhiqi Shen. 2024. LampMark: Proactive Deepfake Detection via Training-Free Landmark Perceptual Watermarks. In *Proceedings of the ACM International Conference on Multimedia (MM)*. 10515–10524.
- [31] Deressa Wodajo and Solomon Atnafu. 2021. Deepfake Video Detection Using Convolutional Vision Transformer. *arXiv preprint arXiv:2102.11126*.
- [32] Valikhuaev Yakhyokhuja. 2024. face-parsing. <https://github.com/zllrunning/face-parsing.PyTorch>.
- [33] Zhiyuan Yan, Taiping Yao, Shen Chen, Yandan Zhao, Xinghe Fu, Junwei Zhu, Donghao Luo, Chengjie Wang, Shouhong Ding, Yunsheng Wu, and Li Yuan. 2024. DF40: Toward Next-Generation Deepfake Detection. In *Proceedings of the*

**Table 8: Ablation results of various losses.**

Method	Protocol-1	
	Seen	Unseen
	ACC	ACC
$\mathcal{L}_{dfa}$	99.60	34.09
$\mathcal{L}_{dfa} + \mathcal{L}_{dfacc}$	99.74	38.48
$\mathcal{L}_{dfa} + \mathcal{L}_{dfacc} + \mathcal{L}_{cmc}$	99.98	60.21
$\mathcal{L}_{dfa} + \mathcal{L}_{dfacc} + \mathcal{L}_{cmc} + \mathcal{L}_{cpc}$	100	64.89
$\mathcal{L}_{dfa} + \mathcal{L}_{dfacc} + \mathcal{L}_{cmc} + \mathcal{L}_{cpc} + \mathcal{L}_{kl}$	<b>100</b>	<b>66.31</b>

*Advances in Neural Information Processing Systems (NIPS)*, Vol. 37. 29387–29434.

- [34] Tianyun Yang, Ziyao Huang, Juan Cao, Lei Li, and Xirong Li. 2022. Deepfake Network Architecture Attribution. In *Proceedings of the AAAI Conference on Artificial Intelligence (AAAI)*. 4662–4670.
- [35] Yaning Zhang, Qiufu Li, Zitong Yu, and Linlin Shen. 2025. Distilled transformers with locally enhanced global representations for face forgery detection. *Pattern Recognition* 161 (2025), 111253.
- [36] Yaning Zhang, Tianyi Wang, Zitong Yu, Zan Gao, Linlin Shen, and Shengyong Chen. 2024. MFCLIP: Multi-modal Fine-grained CLIP for Generalizable Diffusion Face Forgery Detection. *arXiv preprint arXiv:2409.09724* (2024).
- [37] Yaning Zhang, Zitong Yu, Tianyi Wang, Xiaobin Huang, Linlin Shen, Zan Gao, and Jianfeng Ren. 2024. GenFace: A Large-Scale Fine-Grained Face Forgery Benchmark and Cross Appearance-Edge Learning. *IEEE Transactions on Information Forensics and Security* 19 (2024), 8559–8572.

## A Ablation

**Impacts of different losses.** To delve into the contribution of loss functions, we conduct ablations on different losses. The ablation result of various losses is displayed in Table 8. When BMRL is supervised with purely DFA loss, the ACC is 34.09% on unseen generators, but an increase of about 4.4% in ACC could be achieved via adding the DFACC criterion. We argue that it could boost the generalizable deepfake attribution representations via flexible contrastive learning across various generators. At the same time, owing to the addition of the CMC loss, BMRL is improved by 21.8% ACC on unseen generators, demonstrating the effectiveness of language guidance. The introduction of the CPC loss further increases the performance (+4.6%), which shows that the global face parsing features could be valuable prior information for both deepfake detection and attribution. Moreover, due to the integration of the KL loss, our BMRL model achieves an enhancement of 2.5% ACC, which indicates that it is valuable to conduct feature alignment between visual and textual modalities. The incorporation of the five criteria yields the best performance among these losses, indicating that the proposed loss realizes promising results.

**Effects of the margin  $m$  in DFACC loss.** In the DFACC loss, we measure the correlation between generators based on the margin value. We investigate the influence of different margin values on model performance. As shown in Table 9, the ACC score tends to improve with an increase of the margin value, indicating that a larger margin enhances the model ability to distinguish between generators, effectively. Notably, the performance reaches the peak when the margin value is set to 0.7. This suggests that a margin of 0.7 can serve as an optimal value for evaluating the correlation among generators.

**Influences of the factor  $\lambda$  in DFACC loss.** In the DFACC loss, we define the factor  $\lambda$  to balance the loss term between  $\mathcal{L}_{intra}$  and

**Table 9: Influence of margin values in DFACC loss.**

Method		Protocol-1	
		Seen	Unseen
		ACC	ACC
CLIP	m=0.5	88.85	-
	m=0.7	89.07	-
	m=0.9	79.01	-
Ours	m=0.5	97.14	47.01
	m=0.7	<b>100</b>	<b>66.31</b>
	m=0.9	98.65	54.77

**Table 10: Influence of the factor in DFACC loss.**

Method		Testing Set	
		Seen	Unseen
		ACC	ACC
CLIP	$\lambda=0.0$	79.46	-
	$\lambda=0.3$	82.12	-
	$\lambda=0.5$	88.85	-
	$\lambda=0.7$	87.86	-
BMRL	$\lambda=0.0$	93.05	60.18
	$\lambda=0.3$	96.29	63.24
	$\lambda=0.5$	<b>100</b>	<b>66.31</b>
	$\lambda=0.7$	98.03	64.28

$\mathcal{L}_{inter}$ . We study the effect of various factors on model performance. As Table 10 displays, the ACC score rises with the increase of factors, which indicates the effectiveness of flexible metric learning. Specifically, the performance reaches its peak when the weight factor  $\lambda$  is set to 0.5, which means an optimal balance between the two loss terms. We argue that the optimal setting of  $\lambda$  allows the model to learn the most discriminative features, leading to better generalization and more accurate predictions.

## B Visualization

**Visualization of confusion matrix.** We visualize the confusion matrix to observe the prediction results of different models. As shown in Figure 8, MFCLIP achieves lower prediction results compared to BMRL. In detail, some samples may be misclassified, particularly in the following cases: when the data source is identical, such as StyleGAN2 and FSLSD, or as they can be categorized into the same classes, such as the diffusion-based model (e.g., DiffFace and Diffae). By contrast, our BMRL method is capable of decreasing confusion between similar generators while achieving more accurate predictions, i.e., 100% ACC on all generators.

**Visualization of face parsing images.** To show that face parsing images could be regarded as useful prior information, we visualize the parsing image of a real face and that of a fake one generated by various generators. In Figure 7, it is noted that there are evident distinct between authentic facial parsing images and fake ones. In

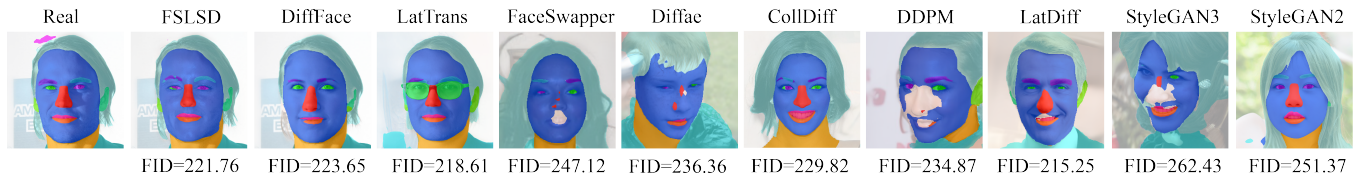


Figure 7: Visualization of face parsing images from various generators.

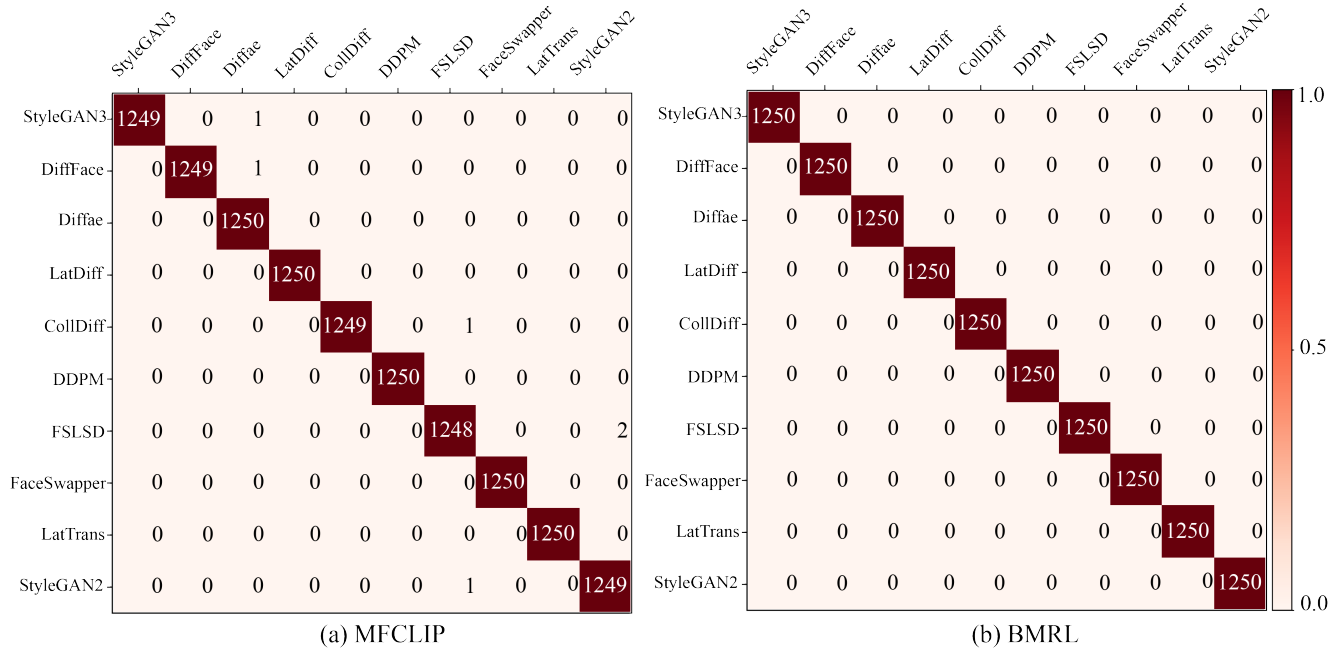


Figure 8: Confusion matrix visualization of various methods.

detail, face images generated by various generators fail to retain complete attribute semantic information. Besides, there are variations in the face parsing maps across images generated by different generators.

We further calculate the FID score of the parsing image from various generators, to observe the distribution discrepancy among them. To ensure a fair and balanced evaluation, we maintain an

equal distribution of pristine and forged face parsing images, i.e., a 1:1 ratio. Specifically, we adopt 10k real images and 10k fake ones for each generator to compute the FID score. The results across various generators are displayed in Figure 7. It is worth noticing that there are distribution differences between different generators, which facilitates DFA.

Received 20 February 2007; revised 12 March 2009; accepted 5 June 2009